

带格式的: 左

1 **Early Holocene ice on the Begguya plateau (Mt. Hunter, Alaska) revealed**
2 **by ice core ¹⁴C age constraints**

3 Ling Fang^{1,§}, Theo M. Jenk^{1,3*}, Dominic Winski⁴, Karl Kreutz⁴, Hanna L. Brooks⁴, Emma
4 Erwin⁴, Erich Osterberg⁵, Seth Campbell⁴, Cameron Wake⁶, Margit Schwikowski^{1,2,3}

5 ¹Laboratory for Environmental Chemistry, Paul Scherrer Institute, CH-5232 Villigen PSI,
6 Switzerland

7 ²Department of Chemistry and Biochemistry, University of Bern, CH-3012 Bern, Switzerland

8 ³Oeschger Centre for Climate Change Research, University of Bern, CH-3012 Bern,
9 Switzerland

10 ⁴Climate Change Institute and School of Earth and Climate Science, University of Maine,
11 Orono, Maine, 04469, USA.

12 ⁵Department of Earth Sciences, Dartmouth College, Hanover, NH 03755

13 ⁶Institute for the Study of Earth, Oceans, and Space, University of New Hampshire, Durham,
14 NH 03824

15 [§]Present address: Shaanxi Key Laboratory of Earth Surface System and Environmental
16 Carrying Capacity, Urban and Environmental Sciences department, Northwest University,
17 Xi'an 710127, China.

18 *Corresponding author

19

20 **Abstract**

21 Investigating North Pacific climate variability during warm intervals prior to the Common Era
22 can improve our understanding of the behavior of ocean-atmosphere teleconnections between
23 low latitudes and the Arctic under future warming scenarios. However, most of the existing ice
24 core records from the Alaska/Yukon region only allow access to climate information covering
25 the last few centuries. Here we present a surface-to-bedrock age scale for a 210-meter long ice
26 core recovered in 2013 from the summit plateau of Begguya (Mt. Hunter; Denali National Park,
27 Central Alaska). Combining dating by annual layer counting with absolute dates from micro-
28 radiocarbon dating, a continuous chronology for the entire ice core archive was established
29 using an ice flow model. Calibrated ^{14}C ages from the deepest section (209.1 m, 7.7 to 9.0 ka
30 cal BP) indicate that basal ice on Begguya is at least of early Holocene origin. A series of
31 samples from a shallower depth interval (199.8 to 206.6 m) were dated with near uniform ^{14}C
32 ages (3 to 5 ka cal BP). Our results suggest this may be related to an increase in annual net
33 snow accumulation rates over this period following the Northern Hemisphere Holocene
34 Climate Optimum (around 8 to 5 ka BP). With absolute dates constraining the timescale for the
35 last > 8 ka, this paleo archive will allow future investigations of Holocene climate and the
36 regional evolution of spatial and temporal changes in atmospheric circulation and hydroclimate
37 in the North Pacific.

38

39 **1 Introduction**

40 Arctic surface temperatures have increased more than twice as fast as global temperature during
41 the early 20th century and since the 1970s (Bengtsson 2004, Tokinaga et al. 2017, Svendsen et
42 al. 2018). Recent modeling results suggest that during the early 20th century, as the Pacific
43 Decadal Oscillation (PDO) transitioned to a positive phase, there was a concomitant deepening
44 of the Aleutian Low that warmed the Arctic through poleward low-level advection of
45 extratropical air (Svendsen et al. 2018). The impact of Pacific multi-decadal variability on
46 Arctic warming has considerable implications for sea ice extent (Screen and Francis 2016), and
47 hence the possible linkage between Arctic amplification, sea ice loss, and enhanced mid-
48 latitude winter variability (Cohen et al. 2014, Francis et al. 2017, Cohen et al. 2018, Screen et
49 al. 2018, Blackport et al. 2019, Cohen et al. 2019). Whether the present positive PDO
50 conditions will persist and contribute to Arctic warming at an even higher rate in the future
51 remains a fundamental question (Svendsen et al. 2018). A longer-term perspective on Pacific
52 decadal variability and the teleconnection between the tropical Pacific, North Pacific, and the
53 Arctic, particularly during warm intervals in the Holocene outside those captured in the
54 instrumental record, would be an important contribution to this problem (e.g., Park et al. 2019).
55 High-mountain ice cores in the North Pacific region have the advantage of sampling
56 atmospheric moisture (e.g., snow), aerosol deposition, and preserving physical characteristics
57 (e.g., melt), all of which can be related to Pacific climate processes (Zdanowicz et al. 2014,
58 Osterberg et al. 2017, Winski et al. 2018), if Holocene (or greater) length records can be
59 recovered.

60 The general timing of deglaciation in Alaska (Brooks Range, Central Alaska Range, and
61 southern Alaska) was determined based on terrestrial cosmogenic radionuclides, lichenometry,
62 and radiocarbon dating to between 10 and 20 ka BP (Dortch 2007). Following the Last Glacial
63 Maximum (LGM), glaciers in the Brooks Range retreated up valley to, or even within, their
64 modern limits by ca. 15 ka (Pendleton et al. 2015). Given the small extent of the Brooks Range
65 glaciers prior to the Holocene thermal maximum, during which some glaciers in southern
66 Alaska disappeared entirely (Barclay et al. 2009), it is possible that the Brooks Range glaciers
67 may have disappeared as well. In the Central Alaska Range, reaching much higher altitudes
68 and considering today's glacier extent, this is rather unlikely. Nevertheless, it is unclear where
69 preserved ice from the early Holocene (or older) can be found in basal layers of these glaciers.
70 Most of the ice cores recovered from the Alaska/Yukon region did not reach bedrock and are
71 thus limited in the time covered, reaching back a few centuries only (Fig. 1). The Prospector

72 Russel Col (PRCol) ice core from Mt. Logan is an exception, having an estimated bottom age
73 of ~20,000 years based on the assumption that the significant depletion in the water stable
74 isotope ratios observed in the very bottom section of the core is a signal of the LGM cold
75 conditions (Fisher et al. 2008). The PRCol chronology is further constrained by a large $\delta^{18}\text{O}$
76 minimum and coeval increases in deuterium excess and Ca^{2+} which are assigned to the 4.2 ka
77 BP event (Walker et al. 2019), and tephra from the large Alaskan eruption of Aniakchak (3.6
78 ka BP, Walker et al. 2019). The PRCol record serves as a Global auxiliary stratotype for the
79 Middle/Late Holocene subdivision boundary (Walker et al. 2019). However, there are no
80 chronologic tie points in the PRCol record prior to the 4.2 ka BP event (Walker et al. 2019).

81 New surface-to-bedrock ice cores were recovered from the Begguya plateau (Mt. Hunter;
82 Denali National Park, Alaska, 62.93°N/151.09°W; Fig. 1) in 2013 at 3900 m elevation (Winski
83 et al. 2017). The two surface-to-bedrock cores (DEN-13A, DEN-13B) reached depths of 211.2
84 and 209.7 meters, respectively. Analysis of the upper 190 meters of DEN-13B (2013 to 810
85 CE) revealed that snow accumulation at the drilling site has doubled since ~1840 CE, coeval
86 with warming of western tropical Pacific sea surface temperatures (Winski et al. 2017) and
87 intensification of the Aleutian Low system (Osterberg et al. 2014, Osterberg et al. 2017). The
88 same core also shows a sixty-fold increase in water equivalent of total annual melt between
89 1850 CE and present, which suggests a summer warming rate of $1.92 \pm 0.31^\circ\text{C}$ per century
90 during the last 100 years in the altitude range of 3900 m (Winski et al. 2018). The Begguya
91 melt layer record is significantly correlated with surface temperatures in the central tropical
92 Pacific through a Rossby-wave like pattern that enhances temperatures over Alaska (Winski et
93 al. 2018). Taken together, these hydroclimate changes are consistent with linkages between
94 Pacific decadal variability and Arctic hydroclimate changes seen in the observational record
95 (Svendsen et al. 2018), and demonstrate that the North Pacific hydroclimate response since
96 1850 CE is unprecedented in the past millennium.

97 The annual layer counting based chronology of the Denali core results in an ice age of
98 1203 ± 41 years at a depth of 190 m (152.8 m w.e.; Winski et al. 2017). Below that depth,
99 annual layering was less consistent due to the loss of seasonal resolution caused by the glacier
100 flow-induced thinning of layers. However, based on previously reported depth-age scales of
101 ice cores from cold, high-elevation glaciers frozen to bedrock, the bottom 20 meters of ice may
102 contain most of the record in terms of time, covering the Holocene and potentially even
103 reaching into the Last Glacial (Uglietti et al. 2016, Licciulli et al. 2020). The Denali ice core
104 therefore provides the possibility of establishing a new Holocene North Pacific hydroclimate

105 record reaching beyond the Common Era, if a precise and absolutely-dated chronology can be
106 established in the bottom 20 meters of the core. The water-insoluble organic carbon (WIOC)
107 and dissolved organic carbon (DOC) ^{14}C -dating method has been validated and applied for
108 multiple mid-latitude ice cores (e.g. Jenk et al. 2009, Uglietti et al. 2016, Hou et al. 2018, Fang
109 et al. 2021). The technique makes use of the transport and deposition of carbonaceous aerosols
110 onto the glacier. Before the industrial period, carbonaceous aerosols were mainly emitted from
111 the living biosphere and from biomass burning. Consequently, this carbon reflects the
112 contemporary atmospheric ^{14}C content (Jenk et al. 2006). After deposition, the WIOC and DOC
113 is incorporated into glacier snow, firn, and ice and undergoes radioactive decay with a half-life
114 of 5730 years (Godwin 1962). Here we report results from ^{14}C analysis of the bottom 60 m of
115 the Denali ice core. These absolute dates extend the existing late Holocene Begguya
116 chronology (Winski et al. 2017), providing the first ~~radiometrically dated~~ high latitude
117 Northern Hemisphere ice core chronology based on absolute dates from radiometric methods.
118 We discuss our results in relation to Holocene ice extent and climate in the North Pacific region.

119 2 Methods

120 2.1 Annual layer counting (ALC)

121 Two surface-to-bedrock ice cores (DEN-13A, DEN-13B) were drilled in 2013 at 3,900 meters
122 elevation (above sea level) from the saddle between the north and middle peaks of Begguya
123 (Mt. Hunter), Alaska (Winski et al. 2017, Osterberg et al. 2017, Winski et al. 2018, Polashenski
124 et al. 2018). The annual layer counting for DEN-13B, ~~conducted by three researchers~~
125 ~~independently~~, was previously published (Winski et al. 2017) and is only briefly described here.
126 The timescale from 2013 to 1777 CE was determined by counting annual oscillations in $\delta^{18}\text{O}$
127 (summer peak), melt layers (summer peak), magnesium (spring peak), dust (spring peak),
128 liquid conductivity (summer peak), ammonium (summer peak) and methanesulfonic acid
129 (MSA; late summer-fall peak), consistent with previous North Pacific ice cores (Yasunari et al.
130 2007, Osterberg et al. 2014, Tsushima et al. 2015). Between 1777 to 1500 CE annual layer
131 counting is based on annual oscillations of $\delta^{18}\text{O}$, δD , dust concentration and liquid conductivity
132 that were measured at higher resolution than the other analytes, while conductivity and dust
133 concentrations were exclusively used to date the ice core from 1500 back to 810 CE. For this
134 study, the counting based on these two parameters has been extended back ~~to 339 CE (see~~
135 ~~Results section 3.2 about Annual layer counting)~~. ~~The Denali ice core chronology is validated~~
136 ~~from 1750–2013 CE by comparing the timing of peaks in sulfate, chloride and conductivity to~~

137 ~~the known dates of explosive volcanic eruptions in time (see section 3.2), as well as by using~~
138 ~~¹³⁷Cs as a stratigraphic indicator of nuclear weapons testing (-).~~

139 2.2 Denali ice core ¹⁴C analysis

140 Sixteen samples were selected from the lower portion of the DEN-13B (Table 1). Because
141 WIOC concentrations at this site were assumed to be low, ice samples of at least 1 kg of mass
142 were cut, aiming for extracted yields of carbon allowing dating with a reasonable uncertainty
143 of 10-20% (> 10 µg C, Uglietti et al. 2016). ~~Samples~~In order to process such large sample
144 volumes, a splitting of the sample for melting was required and the overall filtration time had
145 to be increased. Using artificial ice produced from ultra-pure water, the adapted procedures
146 were tested to reach low blanks similar to the ones previously achieved for smaller samples
147 (Jenk et al., 2009; Uglietti et al., 2016; Fang et al., 2019). Otherwise, the samples for WIOC
148 ~~¹⁴C-dating~~dating were prepared following the protocol described in Uglietti et al. (2016); ~~with~~
149 a brief summary ~~is~~ provided here. In order to remove potential contamination in the outer layer
150 of the ice core, pre-cut samples from the inner part of the core were rinsed with ultra-pure water.
151 After melting, ~~of the contained sample in a pre-cleaned jar (1L, PETG, Semadeni), due to the~~
152 size split in two, the carbonaceous particles contained as impurities in the sample ice were
153 filtered onto a prebaked quartz ~~fibre filters~~fiber filter (Pallflex Tissueqz-2500QAT-UP).
154 Potential particulate carbonates also remaining on the filter were removed by acidifying three
155 times with 0.5 µL of 0.2 M HCl. These initial steps were performed in a class 100 laminar flow
156 box to ensure clean conditions. At the University of Bern (Laboratory for the Analysis of
157 Radiocarbon with AMS - LARA laboratory) the WIOC samples were then combusted in a
158 thermo-optical OC/EC analyzer (Sunset Modeldoc4L, Sunset Laboratory Inc, USA) with a
159 non-dispersive infrared sensor (~~NDIR~~) for CO₂ quantification, using the established Swiss 4S
160 protocol for OC/EC separation (Zhang et al. 2012). Being coupled to a 200 kV compact
161 accelerator mass spectrometer (AMS, mini radiocarbon dating system MICADAS), equipped
162 with a gas ion source and a Gas Interface System (GIS, Ruff et al. 2007, Synal et al. 2007,
163 Szidat et al. 2014), the LARA Sunset-GIS-AMS system (Agrios et al. 2015, Agrios et al. 2017)
164 allowed for final, online ¹⁴C measurements of the CO₂ produced from the WIOC fraction.

165 For the deepest sample from ~209 m depth (Denali 235) the available amount of ice was
166 very limited (~200 g). To ensure sufficient mass of carbon for final AMS analysis, the ¹⁴C
167 dating was performed on the DOC fraction for which a higher concentration compared to the
168 WIOC fraction is expected (Legrand et al. 2013). By a catalyzed UV-Oxidation in a dedicated

169 system, DOC was converted to CO₂ which was then cryogenically trapped and flame sealed in
170 glass ampules for final AMS analysis-~~4~~. [Details can be found in Fang et al. \(2019\).](#)

171 All ¹⁴C results are expressed as fraction modern (F¹⁴C), which is the ¹⁴C/¹²C ratio of the
172 sample divided by the same ratio of the modern standard referenced to the year 1950 CE (NIST
173 standard oxalic acid II, SRM 4990C) both being normalized to -25‰ in δ¹³C to account for
174 isotopic fractionation. Daily AMS calibration was performed using sets of modern (NIST
175 oxalic acid II, SRM 4990C, F¹⁴C = 1.3407 ± 0.0005) and fossil standards (sodium acetate,
176 Sigma-Aldrich, No. 71180, F¹⁴C = 0.0018 ± 0.0005). Final values presented in Table 1 are the
177 AMS F¹⁴C raw data after corrections accounting for constant contamination and cross
178 contamination in the Sunset-GIS-AMS system (or GIS-AMS system for DOC, respectively)
179 and the overall procedural blank contribution introduced from preparation of ice samples to
180 final AMS analysis. F¹⁴C of DOC was corrected for contribution from ¹⁴C in-situ production
181 following Fang et al. (2021). The applied small shift in F¹⁴C of 0.019±0.010, was derived using
182 an in-situ production rate of 260.9 ¹⁴C atoms ~~per gram ice and year~~_{g_{ice}⁻¹ a⁻¹} as ~~the~~ best estimate
183 ~~defined~~ for the site latitude and elevation (Lal et al. 1987, Lal and Jull 1990, Lal 1992), an
184 average accumulation rate of 1.0 ± 0.5 m w.e. ([a best initial guess based on the annual values](#)
185 [from Winski et al. 2017, ranging from 0.2 to 2.0 m w.e. for the time period 810 to 2013 CE](#)),
186 and assuming an average incorporation into DOC of 18±7% (Hoffmann, 2016). ~~To obtain~~[This](#)
187 [correction shifts the calibrated age by 300±200 years older, with uncertainty being fully](#)
188 [propagated as for all other ages. Note that the upper estimate does not exceed the achieved](#)
189 [dating precision defined by the analytical uncertainty \(see Table S1 in the Supplementary\). For](#)
190 [all samples, calibrated radiocarbon ages were derived by calibrating final ~~dates, corrected~~-F¹⁴C](#)
191 [were calibrated values](#) using OxCal v4.4.4 (Ramsey 2021) with IntCal20 (the Northern
192 Hemisphere calibration curve; Reimer et al. 2020) and the OxCal in-built sequence model
193 (Bayesian approach-based deposition model; Ramsey 2008, Ramsey 2017). All calibrated ¹⁴C
194 ages are presented as the 1σ range in years before present (cal BP, with BP referring to the year
195 1950 CE).

196 **3 Results**

197 **3.1 Englacial stratigraphy**

198 Around the Begguya drill site, no folding was observed in ground penetrating radar (GPR) data
199 and the bedrock geometry appears to be uncomplicated (Campbell et al. 2013). New radar data

200 was collected in 2022. Ice thickness, bed topography, and internal stratigraphy of the core site
201 were mapped using GPR (10 MHz center frequency radar system, Blue Systems Integration).
202 Standard processing techniques were applied to the data: clipping stationary periods, applying
203 horizontal stacking, bandpass filtering, and correction for antenna separation (Lilien et al.
204 2020). Data were interpolated for standard trace spacing and then migrated using the SeisUnix
205 sumigtk routine. Clear, visible layering is evident in the majority of the ice column; however,
206 interpretation of the stratigraphy at depth is complicated by sidewall reflections produced from
207 the trough beneath the ice core site. There is no conclusive evidence from this data of either
208 stratigraphic continuity or discontinuity in the bottom-most 10 m of ice (Fig. 2). Future
209 measurements using the millimeter-precision capabilities of autonomous phase sensitive radar
210 (Brennan et al. 2014) would be beneficial to resolve englacial stratigraphy close to the bedrock.

211 3.2 Annual layer counting

212 Annual layer counting (ALC), previously published in Winski et al. 2017 back to 810 CE,
213 [\(section 2.1.\)](#), was extended back to 339 CE ~~(, i.e. for the top 197 meters)-meter~~. The
214 uncertainty in the ALC chronology back to 810 CE was estimated through statistical
215 comparisons among individual layer positions indicated by three individuals (see Winski et al.
216 2017 for details). -By 1900 CE, uncertainty estimates are ± 4 years, increasing to ± 10 years at
217 1500 CE and ± 30 years by 810 CE (190.05 m). Only one individual (DW) performed ALC
218 below 190 m, prohibiting a similar approach to estimate uncertainties, but we estimate ~~and an~~
219 uncertainty of around ± 60 years at 339 CE. These estimates are for ALC only and do not
220 consider additional, constraining information from time horizons. There is no offset between
221 the timescale and inferred volcanic eruptions as indicated by peaks in sulfate, chloride, and
222 conductivity during the 19th and 20th centuries, indicating that an accuracy within ± 2 year
223 throughout the last 200 years is likely. The sulfate and chloride peaks in the 18th century used
224 for chronology validation (inferred as Laki, 1784 CE and Pavlof, 1763 CE) were offset by one
225 year from the ALC chronology. Additionally, ^{137}Cs concentrations in the Denali core strongly
226 peak in the layer assigned to the year 1963 CE, one year after the most extensive atmospheric
227 testing of nuclear weapons, which matches the ^{137}Cs residence time in the atmosphere.

228 3.3 Denali ice core ^{14}C data

229 Air masses leading to precipitation on Begguya (~3900 m asl.) originate predominantly from
230 the Pacific and contain relatively low organic aerosol concentrations (Haque et al. 2016, Choi

231 et al. 2017). The WIOC concentration in the Denali core is thus significantly lower than in ice
232 cores from the Alps. The WIOC concentrations range from 6 to 31 $\mu\text{g C kg}^{-1}$ ice with an average
233 of $13 \pm 7 \mu\text{g C kg}^{-1}$ (Table 1). This is slightly higher than in Greenland snow at Summit (4.6
234 $\mu\text{g C kg}^{-1}$, Hagler et al. 2007), but only about half of the pre-industrial WIOC concentrations
235 in European Alpine ice cores, with $24 \pm 9 \mu\text{g C kg}^{-1}$ (Legrand et al. 2007) and $32 \pm 18 \mu\text{g C}$
236 kg^{-1} (Jenk et al. 2009) from Colle Gnifetti, Monte Rosa, Switzerland and $24 \pm 7 \mu\text{g C kg}^{-1}$ from
237 Fiescherhorn glacier (Jenk et al. 2006). In agreement with findings from previous studies
238 (Legrand et al. 2007), the concentration of DOC ($80 \mu\text{g C kg}^{-1}$), measured in the deepest sample,
239 was significantly higher than the concentration of WIOC.

240 ^{14}C calibration was performed using the OxCal in-built sequence model (Ramsey, 2008,
241 Ramsey 2017; see *Methods*). The assumption that samples are in chronological order allows
242 statistical constraints for the most likely age distribution of the individual samples in the
243 sequence. This assumption of chronological ordering will be discussed below. Samples
244 containing less than $10 \mu\text{g}$ carbon are generally characterized by a wide ~~age-range.~~ This of age
245 probability. A reduction in the dating precision for those samples is expected due to the small
246 carbon amount ~~and the resulting larger analytical uncertainty, related to available for analysis.~~
247 Small amounts on the one hand cause reduced AMS measurement precision (lower analytical
248 AMS precision as well as to a ^{12}C current and less ^{14}C counts) and a lower, thus unfavorable
249 signal-to-noise ratio (i.e. the ratio between size of sample and procedural blank, respectively.)
250 on the other hand. Combined, this leads to a larger overall analytical uncertainty, finally
251 translating into a wider range of possible ages. Although we used a considerable amount of ice
252 for each sample ($\sim 1 \text{ kg}$), the total carbon amount in 5 samples was significantly below this 10
253 $\mu\text{g C}$ threshold recommended to obtain a reliable dating with a final ~~dating~~ uncertainty $< 20\%$
254 for samples older than around 1000 years (Uglietti et al., 2016). These samples will thus not be
255 discussed in the following (but can be found in the supplement material, together with
256 calibration results without sequence constraint).

257 Calibrated ^{14}C ages range from $0.3 \pm 0.3 \text{ ka cal BP}$ at 166.2 m (131.4 m w.e.) depth to
258 $8.4 \pm 0.6 \text{ ka cal BP}$ for the deepest sample (Denali235; 209.1 m or 169.8 m w.e.), the last
259 sample above bedrock (0.6 m), ~~revealing~~. These results show the characteristic exponential
260 increase in age with depth, expected for a cold glacier archive due to the associated ice flow
261 dynamics (e.g. Dansgaard and Johnsen, 1969, also see section 4.1.), and most importantly,
262 reveal ice of early Holocene origin in the Denali ice core (Table 1 and Figure 3). The absolute
263 ages from radiocarbon dating are in agreement with the independently derived ages from the

264 annual layer counting reported in Winski et al (2017), extended back to 339 CE in this study
265 (see *Annual layer counting*). For the youngest sample, Denali183 from a depth of 166.2 m
266 (131.4 m w.e.), and for Denali 214 from 192.6 m (155.0 m w.e.), the 1σ age range is 4-679 a
267 cal BP and 958-1410 a cal BP, respectively; similar to the ~~respective~~corresponding annual layer
268 counting derived ages of 340-380 and 1200-1410 a BP. The 1σ ^{14}C age range for Denali210-
269 211 at 189.5 m (152.3 m w.e.) is 527-930 a cal BP, ~~which is and with a possible age of 930 a~~
270 cal BP only slightly younger than the annual layer counting derived age range of 1020-1200 a
271 BP, ~~but still~~ (in agreement within the 2σ ~~uncertainty~~ range of 317-1174 a cal BP).

272 Samples of indistinguishable ages, with ~~regards~~regard to the achieved dating uncertainty
273 (i.e. analytical precision), were observed in the depth interval from 200.3 to 206.2 m (161.9 to
274 167.2 m w.e.). This interval corresponds to a time period from around 3.2 to 4.3 ka BP. For the
275 respective samples (Denali223, Denali224-225, Denali229-230, Denali231), a low Agreement
276 Index (denoted as *A* in OxCal) resulted for the applied ^{14}C calibration approach. *A* indicates the
277 level of agreement between the probability function derived by the ordinary calibration
278 approach (a priori distribution) and the calibration with additional constraint (a posterior
279 distribution; see OxCal and Ramsey, 2008 and 2017 for more details). Distributions are shown
280 in Figure 3. A value of 100 indicates no alteration in the distribution (100% or unity) while a
281 value lower than 60 indicates a warning to check for the validity of the underlying assumption,
282 i.e. (i) a non-sequential layering of samples, or (ii) the presence of analytical outliers. It is
283 apparent from Figure 3, that the two samples with lowest *A* (<10), Denali 223 and 231, are also
284 characterized by an exceptionally large uncertainty. For the batch of samples with AMS Lab
285 ID BE-10013.1.1 to BE-10022.1.1 (Table 1; see also Supplement Figure S1 and Table S1), the
286 contribution to the final overall uncertainty from AMS analysis only was around twice as much
287 than what typically can be achieved for samples of that carbon ~~size~~mass. For that measurement
288 day, we also observed above average uncertainties for the measured sets of AMS calibration
289 standards, with a slight elevation in the fossil standard value (+0.02 in $F^{14}\text{C}$; see *Method*). This
290 is an indication for non-ideal AMS conditions due to sub-optimal instrument tuning on the one
291 hand, and an elevated, potentially non-stable background that day on the other hand. Thus,
292 neither ^{14}C ages nor the englacial stratigraphy give sufficient evidence to conclude a non-
293 sequential ordering of samples (i.e. an age reversal in the Denali ice core). Additionally, there
294 is evidence from other studies from the region suggesting hydrological changes between
295 around 4 to 2 ka BP (e.g. increased lake levels and precipitation, see *Discussion*), which
296 coincides with the time period in question here. Because increased accumulation rates would

297 lead to a reduced increase in age per unit depth, an unambiguous resolving of the sequence then
298 depends on the achievable analytical uncertainty. Having pushed the limit of the analytical
299 method with the small amounts of carbon available for ^{14}C analysis and considering all the
300 above, we thus exclude assumption (i) and are confident that the applied ^{14}C sequence
301 calibration approach does provide us the most accurate dates.

302 **4 Discussion**

303 **4.1 Denali ice core chronology**

304 Modeling the age scale in high-elevation mountain ice cores can be attempted either by
305 applying rather simple glaciological one-dimensional (1D) flow models (e.g. Nye 1963,
306 Dansgaard and Johnsen 1969, Bolzan 1985) or by much more complex 3D models based on a
307 suit of observational data from glaciological survey (e.g. Campbell et al. 2013, Licciulli et al.
308 2020). Independent of model complexity, age scale modeling, particularly of mountain glaciers,
309 is strongly challenged to provide accurate or even conclusive ages along the profile at a specific
310 point on the glacier (e.g. the ice core drill site; Campbell et al. 2013, Licciulli et al. 2020). This
311 is especially the case close to bedrock, where ice flow can become highly complex, and because
312 past annual net accumulation rates with potential variations over time are unknown. Layers of
313 known age along a glacier depth profile, e.g. from ice core dating, can provide crucial model
314 constraints, allowing free model parameters to be tuned for a best fit between observations and
315 model output. For a defined point, moving along a single axis (bed to surface), 1D models
316 benefit from their simplicity to do so (less parameters). 1D models have been applied for
317 decades to obtain continuous age-depth relationships at sites on polar ice sheets (e.g. Dansgaard
318 and Johnsen 1969), thereby also accounting for past changes in accumulation rates by inverse
319 modelling approaches (e.g. Buiron et al. 2011, Buchardt and Dahl-Jensen 2008). However,
320 applications to sites from high-mountain glaciers are more recent (e.g. Jenk et al. 2009, Uglietti
321 et al. 2016).

322 In the case of the Denali ice core, accurate dating by annual layer counting supported
323 with independent time horizons for the upper two thirds of the core and absolute dated horizons
324 for the deep section of the core (^{14}C dates) are available. Winski et al. 2017 developed a well-
325 defined age scale for the upper part of the core based on annual layer counting supported by
326 distinct time horizons. Since depth-age relationships are less challenging to model in the upper
327 90% of the ice core, because of relatively moderate layer thinning and little if any influence

328 from bedrock, Winski et al. (2017) used a combination of 1D modeling and a 3D glacier flow
329 model developed for this site (Campbell et al. 2013) to determine a significant increase in
330 accumulation rates since around 1850 CE. Therefore, significant changes in net accumulation
331 rates at the Denali ice core drill site should be expected to have also occurred in the more
332 distant past.

333 Due to its simplicity, we used the 1D two-parameter model (2p-model; Bolzan 1985) to
334 provide a first, best estimate for a continuous age-depth relationship from surface to bedrock,
335 building on the available data points presented. The 2p-model is based on a simple analytical
336 expression for the decrease of the annual layer thickness with depth and has two degrees of
337 freedom, the mean annual net accumulation rate b and the thinning parameter p , characterizing
338 the strain rate function; both assumed to be constant over time. Knowing the glacier thickness
339 of 209.7 m from the ice core length (supported by ground penetrating radar data; 170.4 m w.e.)
340 and with all depths converted from meter to meter water equivalent based on the ice core
341 density profile, allowed finding the best solutions for b and p by fitting the model (least squares
342 approach, as described in Fahnestock et al. 2001) through the time horizons in the Denali ice
343 core (Volcanos, ^{137}Cs , ^{14}C). The derived value for p was 0.79 ± 0.01 . The resulting value of b
344 of 1.5 ± 0.1 m w.e. yr^{-1} , representing the mean annual net accumulation rate for the entire period
345 covered by the ice core, is similar to the recently observed 21st century values. It is however
346 significantly higher than the average value of around 0.5 m w.e. yr^{-1} previously determined for
347 the last 810 years (ranging from around 0.3 to 1.5 m w.e. yr^{-1} ; Winski et al. 2017). This is no
348 surprise, considering the likelihood that similar variations may also have occurred further back
349 in time. As a consequence of being constrained by the age of dated layers, the model results
350 are in agreement with the observational data for the total time period covered within the ice
351 column. However, at various depths along the depth profile, a significant offset between model
352 output and data can be observed (Fig. 4a). Again, this is not unexpected, considering the fact
353 that the accumulation rate was kept constant in the model, while significant changes over time
354 are known to have occurred (Winski et al. 2017). In Figure 3a, the effect on model results for
355 variations of b is illustrated (runs with b equal to 0.5, 1.5 and 2 m w.e. yr^{-1} , respectively, with
356 p as determined before).

357 To achieve our final goal, obtaining a continuous age-depth relationship based on the
358 absolute dating presented, we next applied a simple inverse modeling approach. We tightly fit
359 the model to the experimental data, by numerically solving for the exact value of b for each
360 depth with a determined age (p and H as before). To reduce and account for potential noise in

361 the data, an uncertainty weighted three point running mean to obtain the non-steady state values
362 for b was calculated (starting from top, then reversed from bottom, thereby propagating the
363 values for continuity). These values, interpolated for depths between the dated layers, were
364 finally used for model input, yielding a continuous age-depth relationship (Figure 4b and 4c).
365 All uncertainties have been fully propagated throughout calculations (from analysis to
366 modeling). We ~~derive~~derived annual net accumulation rates of 0.5 ± 0.1 m w.e. yr^{-1} at around
367 1000 CE, eventually increasing to a 20th century average value of 1.1 ± 0.2 m w.e. yr^{-1} (Fig. S2).
368 This is in good agreement with what ~~has been~~was determined previously by Winski et al. 2017
369 for the corresponding periods, based on results from different models investigated (for the 3D
370 model considered best: 0.25 m w.e. yr^{-1} around 1000 CE, with models ranging from 0.05 - 0.7
371 m w.e. yr^{-1} , and 1.1 ± 0.3 m w.e. yr^{-1} for the 20th century average, respectively). During the
372 Holocene Climate Optimum (around 8 to 5 ka BP, Kaufman et al. 2016) we ~~obtain~~obtained net
373 accumulation rates of 1.2 ± 0.3 m w.e. yr^{-1} , similar to the average rate observed since 1950 CE,
374 followed by higher rates of 1.7 ± 0.4 m w.e. yr^{-1} from around 4.3 to 3.2 ka BP. Then, the rates
375 decrease over the next 500 to 1000 years to around 0.4 ± 0.2 m w.e. yr^{-1} . See Section 4.3 for
376 further discussion. Our derived age-depth scale results in ages of 9-14 ka BP at 0.5 m above
377 bedrock, strongly suggesting the presence of, at least, early Holocene ice ~~to be present~~ at the
378 Denali ice core drill site.

379 4.2 Ice core chronologies in Eastern Beringia

380 So far, existing ice cores from Eastern Beringia (Table 2) were dated with ages covering less
381 than the last millennium except for the Denali core discussed in this study and the 188 m long
382 PRCol core (Fig. 1) drilled to ~~bedrock~~the bed surface on the summit plateau of Mt. Logan in
383 2001 and 2002. The older part of the PRCol core was dated based on a signal interpreted as the
384 Younger Dryas to Holocene transition (sudden reduction in electrical conductivity coinciding
385 with a drop in $\delta^{18}\text{O}$ and an increase in various chemical species) and a bottom age estimate
386 from an ice flow model of about 20 ka (Fisher et al. 2008). Another ice core from Mt. Logan
387 (King Col, 60.59°N, 140.60°W, 4135 m asl.) was drilled in 2002 reaching a depth of 220.5 m.
388 This core was not dated, but a potential age range of 0.5 to 1.3 ka was estimated based on
389 modeling results (Shiraiwa et al. 2003). The 152 m ice core drilled in 2008 on the McCall
390 Glacier was dated by using a combination of annual layer counting and specific horizons. The
391 upper 37 m of ice date back to 65 years and the full 152 m core was estimated to cover more
392 than 200 years but no actual dating of the lower section was performed (Klein et al. 2016). The

393 Aurora Peak site is located southeast of Mt. Hayes and the ice core was also drilled in 2008.
394 The total ice thickness at the drilling site is 252±10 m, but this core (180.17 m) did not ~~reach~~
395 ~~bedrock~~approach the bed surface. By annual layer counting, the estimated bottom age of the
396 Aurora Peak core is about 274 years (Tsushima et al. 2015). Two cores were collected at
397 Eclipse Icefield in 2002. The chronology of these cores is based on multi-parameter annual
398 layer counting of seasonal oscillations in the stable isotope ($\delta^{18}\text{O}$) and major ion records (Na^+)
399 supported by identification of volcanic horizons. The longest core 2- (345 m) covers the period
400 1000 CE to 2002 CE (Yalcin et al. 2007), but did not reach bedrock. In 2004, a 212 m ice core
401 was drilled from Mt. Wrangell. The ice depth in the summit caldera is probably over 900 m,
402 but the definite bottom has not yet been detected (Benson et al. 2007). For this core, ~~no time~~
403 ~~scale is reported except for~~ a short 12-year record of dust and δD ~~(was reported in~~ Yasunari et
404 al. (2007-), ~~and dating was later extended back to 1981 (23 years) at the depth of 100.1 m~~
405 ~~(Sasaki et al. 2016)~~. The record from Mt. Waddington only covers a period of 1973-2010 CE
406 (Neff et al. 2012). The total length of the Mt. Waddington core is 141 m, but the total ice
407 thickness at the drilling site is about 250 m. The ice core from Bona-Churchill reached bedrock
408 at a depth of 460 m, but the age-depth scale has only been established for the last ~800 years
409 (depth of 399 m); the deepest ice is estimated to exceed 1500 years in age (Porter et al. 2019).

410 Because none of the cores from the Eastern Beringia region was either drilled to
411 ~~bedrock~~the bed surface or the ice close to the bed dated by an absolute dating method, no
412 concluding evidence about the age of the oldest glacier ice preserved in this region existed so
413 far. In this study, we achieved a first, complete and absolute (radiometric) dating by a first
414 application of ^{14}C analysis on a high-latitude Northern Hemisphere ice core from Begguya,
415 which reached ~~down~~the to ~~bedrock~~bed surface. Our results, with calibrated ^{14}C ages of 7.7 to
416 9.0 ka BP close to the bottom (0.61 m above bedrock) and model based indication for
417 potentially even older ice further below (>12 ka BP), clearly indicate that glaciers in this region
418 can be of early Holocene or even Pleistocene origin. ~~This also confirms that at least some~~
419 ~~glacier ice in the Central Alaskan Range, at altitudes as low as 3,900 m a.s.l., survived during~~
420 ~~the Holocene thermal maximum.~~

421 **4.3 Possible implications for Holocene hydroclimate in Eastern Beringia**

422 ~~The mid-Holocene hydroclimate in the North Pacific has been investigated by various studies~~
423 ~~previously carried out in the region (Table 3, Fig. 5). For example, the onset of the regional~~
424 ~~Neoglaciation was estimated to last from around 3.5 to 2.5 ka BP in the Yukon Territory based~~

425 ~~on past tree line variations (Denton and Karlén 1977, Anderson et al. 2005a) and inferred from~~
426 ~~lacustrine records of lake level.~~In recent decades, extensive work has been done in the North
427 ~~Pacific region to characterize Holocene hydroclimate (Table 3, Fig. 5). Following a modest~~
428 ~~Holocene thermal maximum that was 0.2 – 0.5° C warmer than the last millennium average~~
429 ~~(Kaufman et al. 2016), although 1.7° C cooler than present (Porter et al. 2019), glaciers across~~
430 ~~the region advanced synchronously at about 4.5 ka BP (Solomina et al. 2015). This~~
431 ~~Neoglaciation continued through 3.5 to 2.5 ka BP in the Yukon Territory based on past tree~~
432 ~~line variations, lake levels and carbonate oxygen isotopes (Denton and Karlén 1977, L.~~
433 ~~Anderson et al. 2005a). Past tree lines also provided evidence for significant glacier extension~~
434 ~~in the St. Elias Mountains over the period 3.6–3.0 ka BP (a). Denton and Karlén 1977). While~~
435 a mid-Holocene temperature decrease may have played a role, Denton and Karlen (1977)
436 hypothesized that an increase in regional precipitation contributed to the regional
437 Neoglaciation, a conclusion also reached by later studies (e.g. L. Anderson et al., 2011).

438 Concurrent with this Neoglaciation, effective moisture rose across much of the region.
439 Based on pollen reconstructions, Heusser et al. (1985) inferred a doubling of Southern Alaskan
440 mean annual precipitation from around 3.9 to 3.5 ka BP (Fig. 3). Clegg and Hu (2010) found
441 that effective moisture, particularly during winters, increased markedly between 4.0 and 2.5 ka
442 BP. Hansen and Engstrom (1996) ~~suggests~~suggested cooler and wetter conditions in Glacier
443 Bay at around 3.4 ka BP. At Jellybean Lake and Marcella Lake, lake levels were high between
444 2.0–4.0 ka BP (Anderson et al. 2005a, 2005b) which was assigned to changes in the strength
445 and positions of the Aleutian Low (Anderson et al. 2005b), consistent with the more recent
446 interpretation of hydroclimate changes from the Denali ice core ~~(Winski et al. 2017; Osterberg~~
447 ~~et al. 2017).~~(Winski et al. 2017; Osterberg et al. 2017). Records from Mica Lake (Schiff et al.
448 2009) and Sunken Island Lake (Broadman et al. 2020) showed wetter conditions associated
449 with a stronger Aleutian Low at 4 ka and 4.5 BP, respectively. Greenpepper Lake experienced
450 high lake levels from 2–5 ka BP (L. Anderson et al. 2019) and a major shift from moss to sedge
451 occurred at Horse Trail Fen concurrent with a large isotopic anomaly at 3–4 ka BP (Jones et al.
452 2019). At the same time, paleoenvironmental records showed a decrease in wildfire (R.S.
453 Anderson et al. 2006; Kelly et al. 2013).

454 ~~The Denali ice core may provide corroborating evidence for a~~Together, previous work
455 indicates an enhanced flux of moisture into the region, likely associated with a strengthened
456 Aleutian Low, sometime near 4 ka BP (L. Anderson et al. 2016). The Denali ice core may
457 provide corroborating evidence for this mid-Holocene shift in hydroclimate (Table 3, Fig. 5).

458 As presented before, samples of indistinguishable ages, at least for the achieved analytical
459 precision, were observed in the depth interval from 200.3 to 206.2 m (161.9-167.2 m w.e.)
460 corresponding to the modeled time period from 4.3 ± 0.5 to 3.2 ± 0.5 ka BP (see Sections *Denali*
461 *ice core* ^{14}C data and *Denali ice core chronology*). Elevated snow accumulation provides a
462 possible explanation for this clustering of dates and would support many previous studies.
463 While our model results based on ^{14}C ages are consistent with existing interpretations of mid-
464 Holocene changes in regional precipitation, applying other independent dating methods using
465 the remaining parallel ice sections from this depth interval (e.g. from DEN-13B) could be used,
466 and additional geophysical and modeling approaches are needed to rigorously test this
467 hypothesis.

468 Importantly, some hydroclimate studies do not show a shift toward wetter conditions at 4
469 ka BP. On Adak Island, conditions grew cooler and drier at 4.5 ka BP which is consistent with
470 the prevailing interpretation of a stronger Aleutian Low advecting warmer moister air into the
471 Gulf of Alaska and cooler drier air to the western Aleutians (Bailey et al. 2018). Certain sites
472 located to the north of the Alaska or St. Elias ranges also show a drying trend or no major
473 features around 4k (Lasher et al. 2021; Finney et al. 2012; King et al. 2022; Chakraborty et al.
474 2010), emphasizing the idea that orography and rain shadows are critical for controlling the
475 relationship between site precipitation and circulation (Anderson et al. 2016). In fact, Winski
476 et al. (2017), showed that during the instrumental era, Begguya snowfall is highly correlated
477 with precipitation along the Gulf of Alaska, but bears little resemblance to nearby precipitation
478 recorded in interior Alaska; a pattern that seems to hold through the mid-Holocene. We note
479 that the Aleutian Low is a wintertime phenomenon such that the role of summertime
480 precipitation may be an important contributor to some of the observed variability among
481 regional paleorecords. Comparing records with different seasonality or with seasonal
482 resolution will be critical in the future given that most of the isotope-based records listed above
483 are dominated by wintertime Aleutian Low dynamics.

484

485 **5 Conclusion**

486 Although ^{14}C analysis of ice-incorporated carbonaceous aerosols has allowed radiocarbon
487 dating of various high-elevation ice cores from low- and mid-latitudes, this technique has not
488 been applied before ~~in~~for high latitude ice cores because of the generally lower carbon content.

489 The ^{14}C results from the Denali ice core are the first from a high latitude ice core. These were
490 achieved by ~~a slight adaptation of~~ small adaptations in the ice sample preparation procedures
491 for the WIOC ^{14}C -dating method, allowing for which allowed processing of larger ice samples
492 ~~of~~ up to ~~around~~ ≥ 1 kg of ice and the use application of a new technique for ^{14}C dating of the
493 DOC fraction ~~(around three times, which benefits from~~ higher ~~in~~ concentration levels in ice
494 compared to the WIOC fraction (by around a factor of three). Combining dating by annual
495 layer counting to a depth of 197.2 m (159.2 m w.e.; ~1674 years BP or 339 CE, respectively),
496 volcanic tie-points from sulfate, chloride, conductivity, and the new ^{14}C dated horizons, a
497 complete continuous chronology over the entire core was established using a simple inverse
498 ice flow modeling approach. For the overlapping sections, ages based on annual layer counting
499 are confirmed by the agreement with the absolute, radiometric ^{14}C dates.

500 ^{14}C dating of a sample from just 0.61 m above bedrock at around 209 m depth, yielded
501 the first absolute date for near-bedrock ice in the region. Dated to be 7.7 to 9.0 thousand years
502 old, our result clearly indicates this very bottom ice to be of early Holocene age. The additional
503 model results indicate a high likelihood of even older ice below (>12 ka). The old ice at the
504 bottom of the Denali core confirms that at least some glacier ice in the central Alaskan Range
505 survived the Holocene thermal maximum. Future, independent dating methods would be
506 beneficial to further constrain and improve the ~~time scale~~ timescale presented here. Our results
507 show the applicability and great potential of ^{14}C dating on low carbon content samples from
508 North Pacific/Arctic ice cores. While they indicate the Denali ice core to currently be one of
509 the few existing archives in the North Pacific region providing an opportunity to reconstruct
510 Holocene hydroclimate variability, we do expect that similar or even longer paleo ice core
511 records can be recovered from North Pacific glaciers if bedrock can be reached.

512 **Data availability.** All ^{14}C data are available in the supplementary material.

513 **Supplementary material.** Additional Figures and Tables for this article can be found in the
514 Supplementary.

515 **Author contributions.** LF, TMJ and MS performed ^{14}C analysis, evaluation, and the
516 continuous age-depth scale modeling, DW, KK, EO, SC, HLB and CW drilled the core and/or
517 conducted the chemical and physical properties analysis. HLB, DW, and EO identified the
518 annual layers. EE provided the radar image. LF, TMJ, DW, KK and MS wrote the manuscript
519 while all authors contributed to the discussion of the results.

520 **Competing interests.** There is no conflict of interest.

521 **Special issue statement.** This article is part of the special issue “Ice core science at the three
522 poles (CP/TC inter-journal SI)”.

523 **Acknowledgements.** Thanks [go](#) to the Laboratory for the Analysis of Radiocarbon with AMS
524 (LARA) at the University of Bern, especially to Martin Rauber for his help with operating the
525 Sunset-MICADAS system. We thank Denali National Park, Polar Field Services and Talkeetna
526 Air Taxi for providing air support and field assistance, Mike Waszkiewicz for ice core drilling,
527 Brad Markle, Dave Silverstone, Tim Godaire and Elizabeth Burakowski for field assistance,
528 and to more than 25 students for their support in the field and the lab. The work in this
529 manuscript was funded by the U.S. National Science Foundation (AGS-1806422 and AGS-
530 AGS-2002483). FL was supported by State Key Laboratory of Cryospheric Science, Northwest
531 Institute of Eco-Environment and Resources, Chinese Academy Sciences (Grant Number:
532 SKLCS-OP-2021-02).

533

534 **References**

535

- 536 Agrios, K., G. Salazar and S. Szidat, A Continuous-Flow Gas Interface of a Thermal/Optical
537 Analyzer With 14 C AMS for Source Apportionment of Atmospheric Aerosols, Radiocarbon,
538 2017, 59(3), 921-932.
- 539 Agrios, K., G. Salazar, Y.-L. Zhang, C. Uglietti, M. Battaglia, M. Luginbühl, V. G. Ciobanu,
540 M. Vonwiller and S. Szidat, Online coupling of pure O₂ thermo-optical methods–14C AMS
541 for source apportionment of carbonaceous aerosols, Nuclear Instruments and Methods in
542 Physics Research Section B: Beam Interactions with Materials and Atoms, 2015, 361, 288-293.
- 543 Anderson, L., M. B. Abbott, B. P. Finney and M. E. Edwards, Palaeohydrology of the
544 Southwest Yukon Territory, Canada, based on multiproxy analyses of lake sediment cores from
545 a depth transect, The Holocene, 2005a, 15(8), 1172-1183.
- 546 Anderson, L., M. B. Abbott, B. P. Finney and S. J. Burns, Regional atmospheric circulation
547 change in the North Pacific during the Holocene inferred from lacustrine carbonate oxygen
548 isotopes, Yukon Territory, Canada, Quaternary Research, 2005b, 64(1), 21-35.
- 549 [Anderson, L., Finney, B.P. and Shapley, M.D., 2011. Lake carbonate-δ¹⁸O records from the
550 Yukon Territory, Canada: Little Ice Age moisture variability and patterns. Quaternary Science
551 Reviews, 30\(7-8\), 887-898.](#)
- 552 [Anderson, L., M. Berkelhammer, J. A. Barron, B. A. Steinman, B. P. Finney and M. B. Abbott,
553 Lake oxygen isotopes as recorders of North American Rocky Mountain hydroclimate:
554 Holocene patterns and variability at multi-decadal to millennial time scales, Global Planetary
555 Change, 2016, 137, 131-148.](#)
- 556 [Anderson, L., M. Edwards, M. D. Shapley, B. P. Finney and C. Langdon, Holocene
557 thermokarst lake dynamics in northern interior Alaska: the interplay of climate, fire, and
558 subsurface hydrology, Frontiers in Earth Science, 2019, 7, 53.](#)
- 559 [Anderson, R. S., D. J. Hallett, E. Berg, R. B. Jass, J. L. Toney, C. S. de Fontaine and A.
560 DeVolder, Holocene development of boreal forests and fire regimes on the Kenai Lowlands of
561 Alaska, The Holocene, 2006, 16\(6\), 791-803.](#)
- 562 [Bailey, H. L., D. S. Kaufman, H. J. Sloane, A. L. Hubbard, A. C. Henderson, M. J. Leng, H.
563 Meyer and J. M. Welker, Holocene atmospheric circulation in the central North Pacific: A new
564 terrestrial diatom and δ¹⁸O dataset from the Aleutian Islands, Quaternary Science Reviews,
565 2018, 194, 27-38.](#)
- 566 Barclay, D. J., G. C. Wiles and P. E. Calkin, Holocene glacier fluctuations in Alaska,
567 Quaternary Science Reviews, 2009, 28(21-22), 2034-2048.
- 568 Bengtsson, L. S., V. A.; Johannessen, O. M., The Early Twentieth-Century Warming in the
569 Arctic-A Possible Mechanism, Journal of Climate, 2004, 17(20), 4045-4057. DOI:
570 10.1175/1520-0442(2004)017<4045:tetwit>2.0.co;2.
- 571 Benson, C., R. Motyka, S. McNUTT, M. Luethi and M. Truffer, Glacier–volcano interactions
572 in the North Crater of Mt Wrangell, Alaska, Annals of Glaciology, 2007, 45, 48-57.

573 Blackport, R., J. A. Screen, K. van der Wiel and R. Bintanja, Minimal influence of reduced
574 Arctic sea ice on coincident cold winters in mid-latitudes, *Nature Climate Change*, 2019, 9(9),
575 697-704.

576 Bolzan, J. F., Ice flow at the Dome C ice divide based on a deep temperature profile, *Journal*
577 *of Geophysical Research: Atmospheres*, 1985, 90(D5), 8111-8124.

578 Brennan, P. V., L. B. Lok, K. Nicholls and H. Corr, Phase-sensitive FMCW radar system for
579 high-precision Antarctic ice shelf profile monitoring, *IET Radar, Sonar Navigation*, 2014, 8(7),
580 776-786.

581 [Broadman, E., D. S. Kaufman, A. C. Henderson, E. E. Berg, R. S. Anderson, M. J. Leng, S. A.](#)
582 [Stahnke and S. E. Muñoz, Multi-proxy evidence for millennial-scale changes in North Pacific](#)
583 [Holocene hydroclimate from the Kenai Peninsula lowlands, south-central Alaska, *Quaternary*](#)
584 [Science Reviews, 2020, 241, 106420.](#)

585 Buchardt, S. L. and D. Dahl-Jensen, At what depth is the Eemian layer expected to be found at
586 NEEM?, *Annals of glaciology*, 2008, 48, 100-102.

587 Buiron, D., J. Chappellaz, B. Stenni, M. Frezzotti, M. Baumgartner, E. Capron, A. Landais, B.
588 Lemieux-Dudon, V. Masson-Delmotte and M. Montagnat, TALDICE-1 age scale of the Talos
589 Dome deep ice core, East Antarctica, *Climate of the Past*, 2011, 7(1), 1-16.

590 Campbell, S., S. Roy, K. Kreutz, S. A. Arcone, E. C. Osterberg and P. Koons, Strain-rate
591 estimates for crevasse formation at an alpine ice divide: Mount Hunter, Alaska, *Annals of*
592 *glaciology*, 2013, 54(63), 200-208.

593 [Chakraborty, K., S. A. Finkelstein, J. R. Desloges and N. A. Chow, Holocene](#)
594 [paleoenvironmental changes inferred from diatom assemblages in sediments of Kusawa Lake,](#)
595 [Yukon Territory, Canada, *Quaternary Research*, 2010, 74\(1\), 15-22.](#)

596 Choi, Y., T. S. Rhee, J. L. Collett Jr, T. Park, S.-M. Park, B.-K. Seo, G. Park, K. Park and T.
597 Lee, Aerosol concentrations and composition in the North Pacific marine boundary layer,
598 *Atmospheric Environment*, 2017, 171, 165-172.

599 Clegg, B. F. and F. S. Hu, An oxygen-isotope record of Holocene climate change in the south-
600 central Brooks Range, Alaska, *Quaternary Science Reviews*, 2010, 29(7-8), 928-939.

601 Cohen, J., K. Pfeiffer and J. A. Francis, Warm Arctic episodes linked with increased frequency
602 of extreme winter weather in the United States, *Nature communications*, 2018, 9(1), 869.

603 Cohen, J., J. A. Screen, J. C. Furtado, M. Barlow, D. Whittleston, D. Coumou, J. Francis, K.
604 Dethloff, D. Entekhabi and J. Overland, Recent Arctic amplification and extreme mid-latitude
605 weather, *Nature geoscience*, 2014, 7(9), 627-637.

606 Cohen, J., X. Zhang, J. Francis, T. Jung, R. Kwok, J. Overland, T. Ballinger, U. Bhatt, H. Chen
607 and D. Coumou, Divergent consensus on Arctic amplification influence on midlatitude
608 severe winter weather, *Nature Climate Change*, 2019, 1-10.

609 Dansgaard, W. and S. Johnsen, A flow model and a time scale for the ice core from Camp
610 Century, Greenland, *Journal of Glaciology*, 1969, 8(53), 215-223.

611 Denton, G. H. and W. Karlén, Holocene glacial and tree-line variations in the White River
612 Valley and Skolai Pass, Alaska and Yukon Territory, *Quaternary Research*, 1977, 7(1), 63-111.

- 613 Dortch, J. M., Defining the Timing of Glaciation in the Central Alaska Range, Doctoral
614 dissertation, University of Cincinnati, 2007.
- 615 Fahnestock, M., W. Abdalati, S. Luo and S. Gogineni, Internal layer tracing and age-depth-
616 accumulation relationships for the northern Greenland ice sheet, *Journal of Geophysical*
617 *Research: Atmospheres*, 2001, 106(D24), 33789-33797.
- 618 Fang, L., J. Schindler, T. Jenk, C. Uglietti, S. Szidat and M. Schwikowski, Extraction of
619 Dissolved Organic Carbon from Glacier Ice for Radiocarbon Analysis, *Radiocarbon*, 2019,
620 61(3), 681-694.
- 621 Fang, L., T. M. Jenk, T. Singer, S. Hou and M. Schwikowski, Radiocarbon dating of alpine ice
622 cores with the dissolved organic carbon (DOC) fraction, *The Cryosphere*, 2021, 15(3), 1537-
623 1550.
- 624 [Finney, B. P., N. H. Bigelow, V. A. Barber and M. E. Edwards, Holocene climate change and
625 carbon cycling in a groundwater-fed, boreal forest lake: Dune Lake, Alaska, *Journal of*
626 *paleolimnology*, 2012, 48, 43-54.](#)
- 627 Fisher, D., E. Osterberg, A. Dyke, D. Dahl-Jensen, M. Demuth, C. Zdanowicz, J. Bourgeois,
628 R. M. Koerner, P. Mayewski and C. Wake, The Mt Logan Holocene—late Wisconsinan isotope
629 record: tropical Pacific—Yukon connections, *The Holocene*, 2008, 18(5), 667-677.
- 630 Francis, J. A., S. J. Vavrus and J. Cohen, Amplified Arctic warming and mid-latitude weather:
631 new perspectives on emerging connections, *Wiley Interdisciplinary Reviews: Climate Change*,
632 2017, 8(5), e474.
- 633 Godwin, H., Half-life of radiocarbon, *Nature*, 1962, 195(4845), 984.
- 634 Hagler, G. S., M. H. Bergin, E. A. Smith, J. E. Dibb, C. Anderson and E. J. Steig, Particulate
635 and water-soluble carbon measured in recent snow at Summit, Greenland, *Geophysical*
636 *Research Letters*, 2007, 34(16).
- 637 Hansen, B. C. and D. R. Engstrom, Vegetation history of Pleasant Island, southeastern Alaska,
638 since 13,000 yr BP, *Quaternary Research*, 1996, 46(2), 161-175.
- 639 Haque, M. M., K. Kawamura and Y. Kim, Seasonal variations of biogenic secondary organic
640 aerosol tracers in ambient aerosols from Alaska, *Atmospheric Environment*, 2016, 130, 95-104.
- 641 Hayward, C., High spatial resolution electron probe microanalysis of tephra and melt
642 inclusions without beam-induced chemical modification. *The Holocene*, 2012, 22(1), 119–125.
643 <https://doi.org/10.1177/0959683611409777>
- 644 Heusser, C. J., L. Heusser and D. Peteet, Late-Quaternary climatic change on the American
645 North Pacific coast, *Nature*, 1985, 315(6019), 485-487.
- 646 Hou, S., T. M. Jenk, W. Zhang, C. Wang, S. Wu, Y. Wang, H. Pang and M. Schwikowski, Age
647 ranges of the Tibetan ice cores with emphasis on the Chongce ice cores, western Kunlun
648 Mountains, *The Cryosphere*, 2018, 12(7), 2341-2348.
- 649 Iverson, N. A., D. Kaltefleiter, N. W. Dunbar, A. Kurbatov and M. Yates, Advancements and best
650 practices for analysis and correlation of tephra and cryptotephra in ice, *Quaternary*
651 *Geochronology*, 2017, 40, 45-55.

652 Jenk, T. M., S. Szidat, M. Schwikowski, H. W. Gaggeler, S. Brutsch, L. Wacker, H. A. Synal
653 and M. Saurer, Radiocarbon analysis in an Alpine ice core: record of anthropogenic and
654 biogenic contributions to carbonaceous aerosols in the past (1650-1940), *Atmospheric
655 Chemistry and Physics*, 2006, 6, 5381-5390.

656 Jenk, T. M., S. Szidat, D. Bolius, M. Sigl, H. W. Gaeggeler, L. Wacker, M. Ruff, C. Barbante,
657 C. F. Boutron and M. Schwikowski, A novel radiocarbon dating technique applied to an ice
658 core from the Alps indicating late Pleistocene ages, *Journal of Geophysical Research:
659 Atmospheres*, 2009, 114(D14).

660 [Jones, M. C., L. Anderson, K. Keller, B. Nash, V. Littell, M. Wooller and C. A. Jolley, An
661 assessment of plant species differences on cellulose oxygen isotopes from two Kenai Peninsula,
662 Alaska peatlands: Implications for hydroclimatic reconstructions, *Frontiers in Earth Science*,
663 2019, 7, 25.](#)

664 Kaufman, D. S., Y. L. Axford, A. C. Henderson, N. P. McKay, W. W. Oswald, C. Saenger, R.
665 S. Anderson, H. L. Bailey, B. Clegg and K. Gajewski, Holocene climate changes in eastern
666 Beringia (NW North America)—A systematic review of multi-proxy evidence, *Quaternary
667 Science Reviews*, 2016, 147, 312-339.

668 [Kelly, R., M. L. Chipman, P. E. Higuera, I. Stefanova, L. B. Brubaker and F. S. Hu, Recent
669 burning of boreal forests exceeds fire regime limits of the past 10,000 years, *Proceedings of
670 the National Academy of Sciences*, 2013, 110\(32\), 13055-13060.](#)

671 [King, A. L., L. Anderson, M. Abbott, M. Edwards, M. S. Finkenbinder, B. Finney and M. J.
672 Wooller, A stable isotope record of late Quaternary hydrologic change in the northwestern
673 Brooks Range, Alaska \(eastern Beringia\), *Journal of Quaternary Science*, 2022, 37\(5\), 928-943.](#)

674 Klein, E., M. Nolan, J. McConnell, M. Sigl, J. Cherry, J. Young and J. Welker, McCall Glacier
675 record of Arctic climate change: Interpreting a northern Alaska ice core with regional water
676 isotopes, *Quaternary Science Reviews*, 2016, 131, 274-284.

677 Lal, D., *Cosmogenic in situ radiocarbon on the earth. Radiocarbon After Four Decades*,
678 Springer, 1992, 146-161.

679 Lal, D., K. Nishiizumi and J. Arnold, In situ cosmogenic ^3H , ^{14}C , and ^{10}Be for determining the
680 net accumulation and ablation rates of ice sheets, *Journal of Geophysical Research: Solid Earth*,
681 1987, 92(B6), 4947-4952.

682 Lal, D. and A. Jull, On determining ice accumulation rates in the past 40,000 years using in
683 situ cosmogenic ^{14}C , *Geophysical Research Letters*, 1990, 17(9), 1303-1306.

684 [Lasher, G. E., M. B. Abbott, L. Anderson, L. Yasarer, M. Rosenmeier and B. P. Finney,
685 Holocene hydroclimatic reorganizations in northwest Canada inferred from lacustrine
686 carbonate oxygen isotopes, *Geophysical Research Letters*, 2021, 48\(16\), e2021GL092948.](#)

687 Legrand, M., S. Preunkert, M. Schock, M. Cerqueira, A. Kasper-Giebl, J. Afonso, C. Pio, A.
688 Gelencsér and I. Dombrowski-Etchevers, Major 20th century changes of carbonaceous aerosol
689 components (EC, WinOC, DOC, HULIS, carboxylic acids, and cellulose) derived from Alpine
690 ice cores, *Journal of Geophysical Research*, 2007, 112(D23). DOI: 10.1029/2006jd008080.

691 Legrand, M., S. Preunkert, B. May, J. Guilhermet, H. Hoffman and D. Wagenbach, Major 20th
692 century changes of the content and chemical speciation of organic carbon archived in Alpine

693 ice cores: Implications for the long-term change of organic aerosol over Europe, *Journal of*
694 *Geophysical Research: Atmospheres*, 2013, 118(9), 3879-3890.

695 Licciulli, C., P. Bohleber, J. Lier, O. Gagliardini, M. Hoelzle and O. Eisen, A full Stokes ice-
696 flow model to assist the interpretation of millennial-scale ice cores at the high-Alpine drilling
697 site Colle Gnifetti, Swiss/Italian Alps, *Journal of Glaciology*, 2020, 66(255), 35-48.

698 Lilien, D. A., B. H. Hills, J. Driscoll, R. Jacobel and K. Christianson, ImpDAR: an open-source
699 impulse radar processor, *Annals of Glaciology*, 2020, 61(81), 114-123.

700 Neff, P. D., E. J. Steig, D. H. Clark, J. R. McConnell, E. C. Pettit and B. Menounos, Ice-core
701 net snow accumulation and seasonal snow chemistry at a temperate-glacier site: Mount
702 Waddington, southwest British Columbia, Canada, *Journal of Glaciology*, 2012, 58(212),
703 1165-1175. DOI: 10.3189/2012JoG12J078.

704 Nye, J., On the theory of the advance and retreat of glaciers, *Geophysical Journal International*,
705 1963, 7(4), 431-456.

706 Osterberg, E. C., P. A. Mayewski, D. A. Fisher, K. J. Kreutz, K. A. Maasch, S. B. Sneed and
707 E. Kelsey, Mount Logan ice core record of tropical and solar influences on Aleutian Low
708 variability: 500–1998 A.D, *Journal of Geophysical Research: Atmospheres*, 2014, 119(19),
709 2014JD021847. DOI: 10.1002/2014JD021847.

710 Osterberg, E. C., D. A. Winski, K. J. Kreutz, C. P. Wake, D. G. Ferris, S. Campbell, D. Introne,
711 M. Handley and S. Birkel, The 1200 year composite ice core record of Aleutian Low
712 intensification, *Geophysical Research Letters*, 2017, 44(14), 7447-7454. DOI:
713 10.1002/2017GL073697.

714 Park, H.-S., S.-J. Kim, A. L. Stewart, S.-W. Son and K.-H. Seo, Mid-Holocene Northern
715 Hemisphere warming driven by Arctic amplification, *Science Advances*, 2019, 5(12),
716 eaax8203.

717 Pendleton, S. L., E. G. Ceperley, J. P. Briner, D. S. Kaufman and S. Zimmerman, Rapid and
718 early deglaciation in the central Brooks Range, Arctic Alaska, *Geology*, 2015, 43(5), 419-422.

719 Polashenski, D. J., E. C. Osterberg, B. G. Koffman, D. Winski, K. Stamieszkin, K. J. Kreutz,
720 C. P. Wake, D. G. Ferris, D. Introne and S. Campbell, Denali ice core methanesulfonic acid
721 records North Pacific marine primary production, *Journal of Geophysical Research:*
722 *Atmospheres*, 2018, 123(9), 4642-4653.

723 Porter, S. E., E. Mosley-Thompson and L. G. Thompson, Ice core $\delta^{18}\text{O}$ record linked to
724 Western Arctic sea ice variability, *Journal of Geophysical Research: Atmospheres*, 2019,
725 124(20), 10784-10801.

726 Ramsey, C. B., Deposition models for chronological records, *Quaternary Science Reviews*,
727 2008, 27(1-2), 42-60.

728 Ramsey, C. B., Methods for summarizing radiocarbon datasets, *Radiocarbon*, 2017, 59(6),
729 1809-1833.

730 Ramsey, C. B., OxCal 4.4.4 calibration program. Website: [https://c14.arch.ox.ac.](https://c14.arch.ox.ac.uk/oxcal/OxCal.html)
731 [uk/oxcal/OxCal.html](https://c14.arch.ox.ac.uk/oxcal/OxCal.html), 2021.

- 732 Reimer, P. J., W. E. Austin, E. Bard, A. Bayliss, P. G. Blackwell, C. B. Ramsey, M. Butzin, H.
733 Cheng, R. L. Edwards and M. Friedrich, The IntCal20 Northern Hemisphere radiocarbon age
734 calibration curve (0–55 cal kBP), *Radiocarbon*, 2020, 62(4), 725-757.
- 735 Ruff, M., L. Wacker, H. Gäggeler, M. Suter, H.-A. Synal and S. Szidat, A gas ion source for
736 radiocarbon measurements at 200 kV, *Radiocarbon*, 2007, 49(2), 307-314.
- 737 [Sasaki, H., Matoba, S., Shiraiwa, T. and Benson, C.S., Temporal variation in iron flux](#)
738 [deposition onto the Northern North Pacific reconstructed from an ice core drilled at Mount](#)
739 [Wrangell, Alaska, SOLA, 2016, 12, 287-290. DOI:10.2151/sola.2016-056.](#)
- 740 [Schiff, C. J., D. S. Kaufman, A. P. Wolfe, J. Dodd and Z. Sharp, Late Holocene storm-trajectory](#)
741 [changes inferred from the oxygen isotope composition of lake diatoms, south Alaska, Journal](#)
742 [of Paleolimnology, 2009, 41, 189-208.](#)
- 743 Screen, J. A. and J. A. Francis, Contribution of sea-ice loss to Arctic amplification is regulated
744 by Pacific Ocean decadal variability, *Nature Climate Change*, 2016, 6(9), 856.
- 745 Screen, J. A., C. Deser, D. M. Smith, X. Zhang, R. Blackport, P. J. Kushner, T. Oudar, K. E.
746 McCusker and L. Sun, Consistency and discrepancy in the atmospheric response to Arctic sea-
747 ice loss across climate models, *Nature Geoscience*, 2018, 11(3), 155-163.
- 748 [Shiraiwa, T., Goto-Azuma, K., Matoba, S., Yamasaki, T., Segawa, T., Kanamori, S., Matsuoka,](#)
749 [K. and Fujii, Y., Ice core drilling at King Col, Mount Logan 2002, Bulletin of Glaciological](#)
750 [Research, 2003, 20, 57-63.](#)
- 751 Solomina, O. N., R. S. Bradley, D. A. Hodgson, S. Ivy-Ochs, V. Jomelli, A. N. Mackintosh, A.
752 Nesje, L. A. Owen, H. Wanner and G. C. Wiles, Holocene glacier fluctuations, *Quaternary*
753 *Science Reviews*, 2015, 111, 9-34.
- 754 Svendsen, L., N. Keenlyside, I. Bethke, Y. Gao and N.-E. Omrani, Pacific contribution to the
755 early twentieth-century warming in the Arctic, *Nature Climate Change*, 2018, 8(9), 793.
- 756 Synal, H.-A., M. Stocker and M. Suter, MICADAS: a new compact radiocarbon AMS system,
757 *Nuclear Instruments and Methods in Physics Research Section B: Beam Interactions with*
758 *Materials and Atoms*, 2007, 259(1), 7-13.
- 759 Szidat, S., G. A. Salazar, E. Vogel, M. Battaglia, L. Wacker, H.-A. Synal and A. Türlér, ^{14}C
760 analysis and sample preparation at the new Bern Laboratory for the Analysis of Radiocarbon
761 with AMS (LARA), *Radiocarbon*, 2014, 56(2), 561-566.
- 762 Tokinaga, H., S.-P. Xie and H. Mukougawa, Early 20th-century Arctic warming intensified by
763 Pacific and Atlantic multidecadal variability, *Proceedings of the National Academy of Sciences*,
764 2017, 114(24), 6227-6232.
- 765 [Tsushima, A., S. Matoba, T. Shiraiwa, S. Okamoto, H. Sasaki, D. J. Solie and K. Yoshikawa,](#)
766 [Reconstruction of recent climate change in Alaska from the Aurora Peak ice core, central](#)
767 [Alaska, Clim. Past, 2015, 11\(2\), 217-226. DOI: 10.5194/ep11-217-2015.:](#) A study on
768 [reconstruction of paleo-environmental changes in the northern North Pacific region from an](#)
769 [alpine ice core, A Doctor's thesis, Hokkaido University, 78 pp.,](#)
770 [https://doi.org/10.14943/doctoral.k11790, 2015.](https://doi.org/10.14943/doctoral.k11790)

771 Uglietti, C., A. Zapf, T. M. Jenk, M. Sigl, S. Szidat, G. Salazar and M. Schwikowski,
772 Radiocarbon dating of glacier ice: overview, optimisation, validation and potential, *The*
773 *Cryosphere*, 2016, 10(6), 3091-3105. DOI: 10.5194/tc-10-3091-2016.

774 Walker, M., M. J. Head, J. Lowe, M. Berkelhammer, S. Björck, H. Cheng, L. C. Cwynar, D.
775 Fisher, V. Gkinis and A. Long, Subdividing the Holocene Series/Epoch: formalization of
776 stages/ages and subseries/subepochs, and designation of GSSPs and auxiliary stratotypes,
777 *Journal of Quaternary Science*, 2019, 34(3), 173-186.

778 Winski, D., E. Osterberg, D. Ferris, K. Kreutz, C. Wake, S. Campbell, R. Hawley, S. Roy, S.
779 Birkel, D. Introne and M. Handley, Industrial-age doubling of snow accumulation in the Alaska
780 Range linked to tropical ocean warming, *Scientific Reports*, 2017, 7(1), 17869. DOI:
781 10.1038/s41598-017-18022-5.

782 Winski, D., E. Osterberg, K. Kreutz, C. Wake, D. Ferris, S. Campbell, M. Baum, A. Bailey, S.
783 Birkel and D. Introne, A 400-Year Ice Core Melt Layer Record of Summertime Warming in
784 the Alaska Range, *Journal of Geophysical Research: Atmospheres*, 2018, 123(7), 3594-3611.

785 Yalcin, K., C. P. Wake, K. J. Kreutz, M. S. Germani and S. I. Whitlow, Ice core paleovolcanic
786 records from the St. Elias Mountains, Yukon, Canada, *Journal of Geophysical Research:*
787 *Atmospheres*, 2007, 112(D8).

788 Yasunari, T. J., T. Shiraiwa, S. Kanamori, Y. Fujii, M. Igarashi, K. Yamazaki, C. S. Benson
789 and T. Hondoh, Intra-annual variations in atmospheric dust and tritium in the North Pacific
790 region detected from an ice core from Mount Wrangell, Alaska, *Journal of Geophysical*
791 *Research: Atmospheres*, 2007, 112(D10).

792 Zdanowicz, C., D. Fisher, J. Bourgeois, M. Demuth, J. Zheng, P. Mayewski, K. Kreutz, E.
793 Osterberg, K. Yalcin and C. Wake, Ice cores from the St. Elias Mountains, Yukon, Canada:
794 their significance for climate, atmospheric composition and volcanism in the North Pacific
795 region, *Arctic*, 2014, 35-57.

796 Zhang, Y. L., N. Perron, V. G. Ciobanu, P. Zotter, M. C. Minguillón, L. Wacker, A. S. H.
797 Prévôt, U. Baltensperger and S. Szidat, On the isolation of OC and EC and the optimal strategy
798 of radiocarbon-based source apportionment of carbonaceous aerosols, *Atmospheric Chemistry*
799 *and Physics*, 2012, 12, 10841-10856.

800

801

802 **Table 1** ^{14}C results of the Denali ice core samples (DEN-13B), given as F^{14}C , ^{14}C ages, and calibrated ^{14}C ages. For ^{14}C calibration, chronological layering was
803 assumed (sequential deposition, see main text). Samples were dated using the WIOC fraction, except for section 235 in which the DOC fraction was analysed.
804 Numbers of the carbon amount available for ^{14}C AMS analysis as well as the concentration of WIOC (DOC) in the sample are also provided. Additionally
805 shown is the range of the dating based on ALC (range from top to bottom depth of section) and the final age scale (inverse ice flow model).

Sample ID	AMS Lab ID	Depth (m)	Mid Depth (m w.e.)	Carbon amount ($\mu\text{g C}$)	WIOC ($\mu\text{g kg}^{-1}$)	F^{14}C (1σ)	^{14}C age (a BP, 1σ)	Calibrated ^{14}C age (a cal BP, 1σ range)	Final age scale (a BP)	ALC (a BP)
Denali164	BE-10013.1.1	148.6-149.4	115.90	7.0	6.2	0.910 ± 0.058	758 ± 513	-*	160-180	150-180
Denali183	BE-10015.1.1	165.7-166.6	131.40	10.8 811	10.1	0.921 ± 0.042	661 ± 367	4-679	350-370	340-380
Denali209	BE-10016.1.1	187.8-188.7	151.16	9.2	9.8	0.826 ± 0.044	1536 ± 428	-*	1010-1060	980-1090
Denali210-211	BE-8997.1.1	188.7-190.3	152.29	10.8 811	20.0	0.922 ± 0.033	652 ± 288	527-930	1080-1130	1030-1190
Denali214	BE-10017.1.1	192.1-192.9	155.00	13.7 714	11.8	0.831 ± 0.036	1487 ± 348	958-1410	1160-1420	1230-1380
Denali215-216	BE-8998.1.1	193.0-194.7	156.17	8.89	12.0	0.925 ± 0.039	626 ± 339	-*	1200-1560	1290-1500
Denali217	BE-10018.1.1	194.7-195.5	157.33	6.7	6.1	0.731 ± 0.054	2517 ± 594	-*	1280-1710	1400-1560
Denali219-220	BE-8615.1.1	196.4-197.3	159.31	12.0	16.8	0.841 ± 0.026	1391 ± 248	1242-1706	1560-1970	>1420
Denali223	BE-10019.1.1	199.8-200.7	161.93	21.4	17.3	0.608 ± 0.029	3997 ± 383	3079-3469	2180-2890	-
Denali224-225	BE-11923.1.1	200.7-202.3	163.06	33.7 934	17.5	0.653 ± 0.010	3423 ± 123	3257-3530	2470-3510	-
Denali228	BE-10020.1.1	203.5-204.2	165.11	8.79	10.0	0.627 ± 0.043	3750 ± 552	-*	2860-3850	-
Denali229-230	BE-11924.1.1	204.2-205.7	166.09	38.7 639	20.0	0.691 ± 0.009	2969 ± 105	3305-3566	3040-4040	-
Denali231	BE- 10021.1.1 206.6	205.7-206.6 206.6	167.18 168.26	11.3 54.855	11.5 30.8	0.523± 0.629 ± 0.037 0.008	5207 ± 569 3724 ± 102	3840-4263 4067-4407	3540-4560 4520-5430	-
Denali232-233	BE-11925.1.1	206.6-208.1	168.26	54.855	30.8	0.629 ± 0.008	3724 ± 102	4067-4407	4520-5430	-
Denali234	BE-10022.1.1	208.1-208.8	169.23	9.81 0	11.7	0.378 ± 0.043	7814 ± 918	7264-8406	6270-9650	-
Denali235 [#]	BE-12465.1.1	208.8-209.4	169.83	20.7 721	80.3 _{DOC}	(0.437 ± 0.025)	6649 ± 447			

0.418 ± 7007 ± 520 7737-8987[§] 8920-13140 -
0.027[§]

806 ^{*}Following recommendations, samples with a carbon mass of significantly less than 10 µg C were not considered (Uglietti et al. 2016).

807 [#]Results from the DOC fraction.

808 [§]After correction for in-situ ¹⁴C production (Fang et al. 2021; see main text).

809

810 **Table 2** Overview of existing North Pacific ice cores.

Site	Year of drilling (CE)	Latitude (°N)	Longitude (°W)	Elevation (m asl.)	Depth (m)	Reported time span (a)
McCall Glacier ^a	2008	69.17	143.47	2310	152	>200
Aurora Peak ^b	2008	63.52	146.54	2825	180	~274
Begguya ^c	2013	62.56	151.05	3900	208	>8'000
Mt. Wrangell ^d	2004	62.00	144.00	4100 4317	212	-1223
Bona-Churchill ^e	2002	61.40	141.42	4420	461	~800
Mt. Logan PRCol ^f	2001-2002	60.59	140.50	5340	188	~20'000
Eclipse Icefield ^g	2002	60.51	139.47	3017	345	~1'000
Mt. Waddington ^h	2010	51.38	125.26	3000	141	~40

811

812 ^aMcCall Glacier (Klein et al. 2016), ^bAurora Peak (Tsushima ~~et al.~~ 2015), ^cBegguya (this study), ^dMt. Wrangell (Yasunari et al. 2007); [Sasaki et al., 2016](#),

813 ^eBona-Churchill (Porter et al. 2019), ^fMt. Logan (Fisher et al. 2008), ^gEclipse Icefield (Yalcin et al. 2007), ^hMt. Waddington (Neff et al. 2012)

814 **Table 3** Regional paleoclimate events.

Location	Reference	Paleoclimate events	Time (ka BP)
Begguya	this This study	Elevated net accumulation rates	4.3±0.5 to 3.2±0.5
Yukon Territory	Denton and Karlén 1977; L. Anderson et al. 2005 2005b	Neoglaciation	3.5 to 2.5
St. Elias Mountains	Denton and Karlén 1977	Glacier extension	3.6 to 3.0
Alaska	Solomina et al. 2015	Glacier extension	3.5 to 3.0

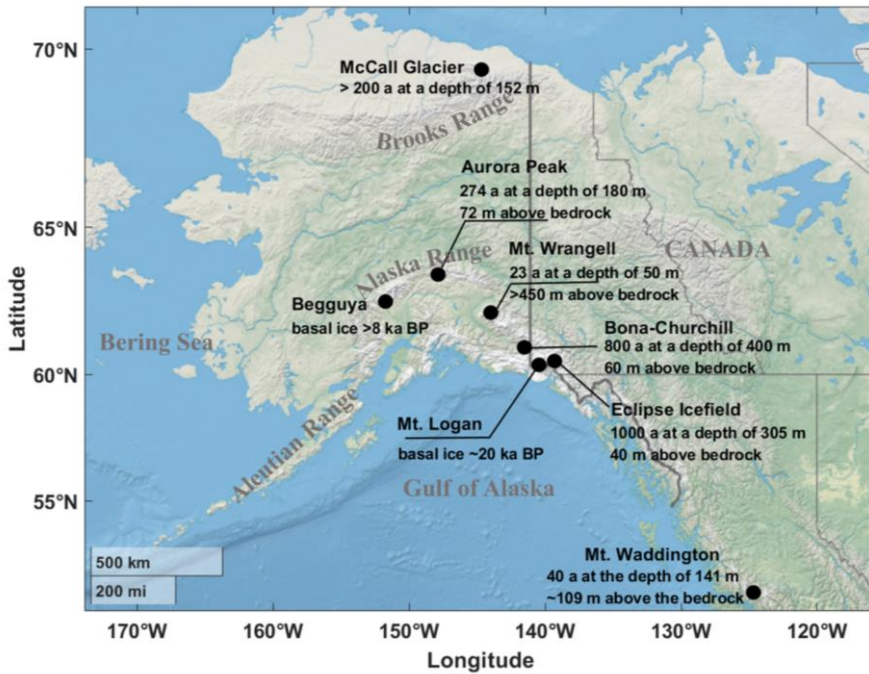
815

816 -

<u>Marcella Lake</u>	<u>L. Anderson et al. 2005b</u>	<u>High lake levels</u>	<u>4.0 to 2.0</u>
<u>Greenpepper Lake</u>	<u>L. Anderson et al. 2019</u>	<u>High lake levels</u>	<u>5.0 to 2.0</u>
<u>Jellybean Lake</u>	<u>L. Anderson et al. 2005a</u>	<u>Intensified Aleutian Low</u>	<u>4.0 to 2.0</u>
<u>Mica Lake</u>	<u>Schiff et al. 2009</u>	<u>Intensified Aleutian Low</u>	<u>4.0 ±0.5</u>
<u>Sunken Island Lake</u>	<u>Broadman et al. 2020</u>	<u>Intensified Aleutian Low</u>	<u>5.0-4.0</u>
<u>Takahula Lake</u>	<u>Clegg and Hu 2010</u>	<u>High effective moisture</u>	<u>4.0 to 2.5</u>
<u>Horse Trail Fen</u>	<u>Jones et al 2019</u>	<u>Isotopic anomaly</u>	<u>4.0 to 3.0</u>
<u>Southern Alaskan</u>	<u>Heusser et al. 1985</u>	<u>Precipitation increases</u>	<u>3.9 to 3.5</u>
<u>Kenai Lowlands</u>	<u>R.S. Anderson et al. 2006</u>	<u>Decrease in wildfire</u>	<u>5.5 to 4.5</u>
<u>Yukon Flats</u>	<u>Kelly et al. 2013</u>	<u>Decrease in wildfire</u>	<u>5.0 to 4.0</u>

817

818



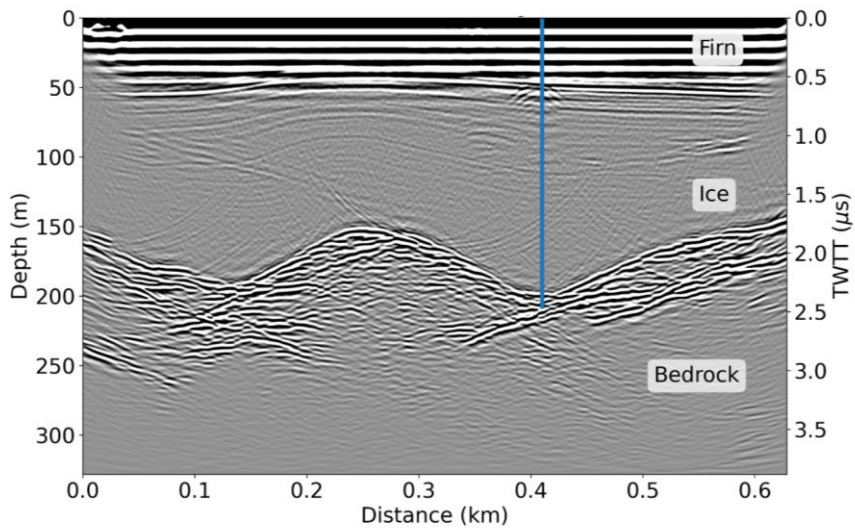
819

820

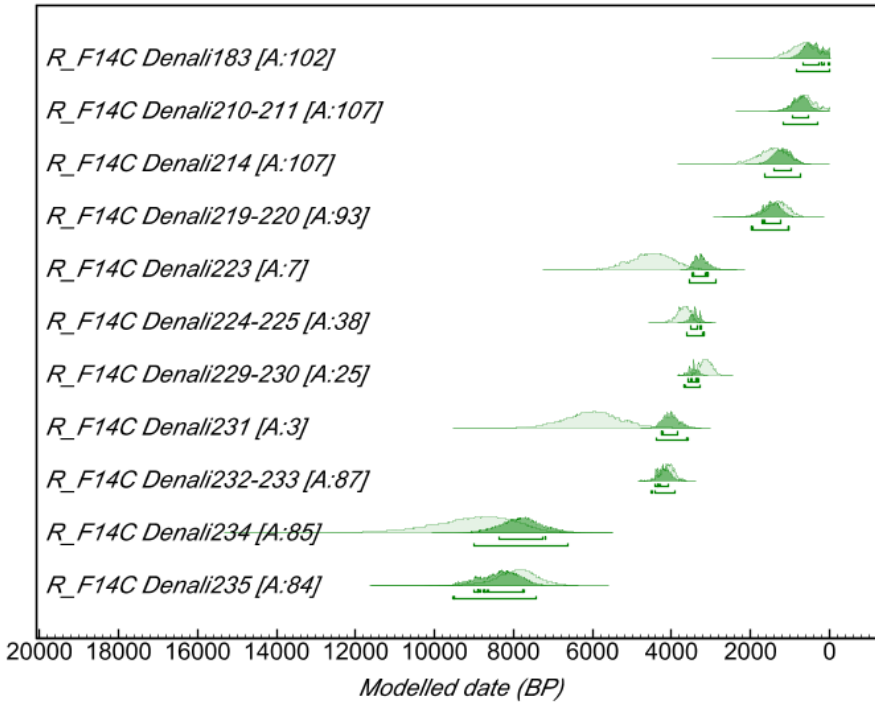
821 **Figure 1** Location map of North Pacific ice core sites and the age of the oldest ice dated from
 822 each location: Begguya (Mt. Hunter; this study), McCall Glacier (Klein et al. 2016), Aurora
 823 Peak (Tsushima *et al.* 2015), Mt. Wrangell (Yasunari et al. 2007), Bona-Churchill (Porter et al.
 824 2019), Mt. Logan (Fisher et al. 2008), Eclipse Icefield (Yalcin et al. 2007), and Mt. Waddington
 825 (Neff et al. 2012). The map was produced using MATLAB (R2019b).

826

827



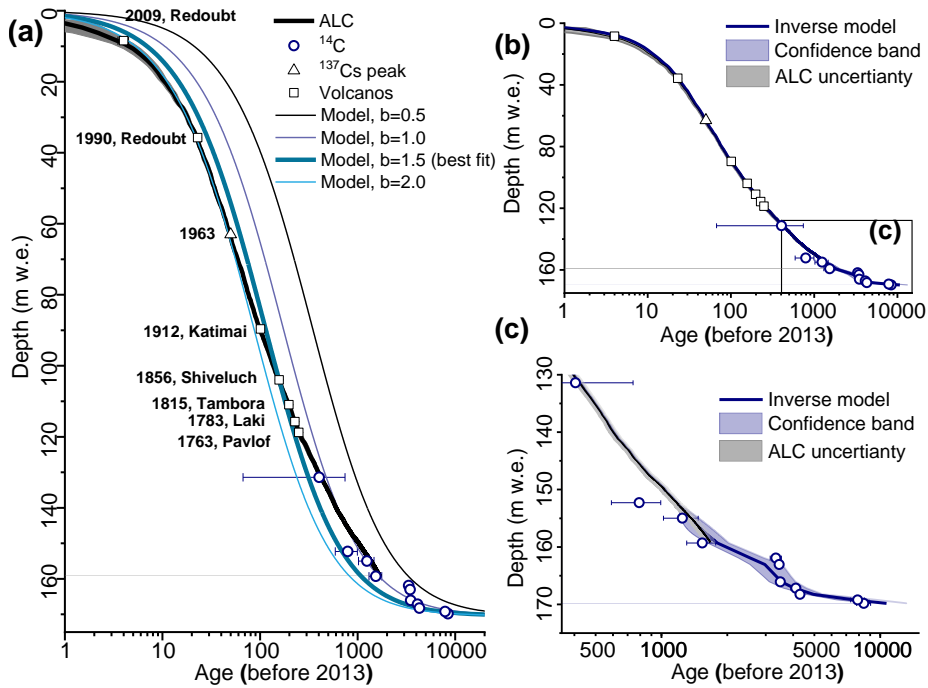
828
 829 **Figure 2** Ground penetrating radar profile collected with 10 MHz BSI radar across the Begguya
 830 plateau in 2022. Standard processing techniques were applied to the data using ImpDAR
 831 (Lilien et al. 2020). The Two-Way Travel Time (TWTT) is plotted on the y-axis on the right
 832 side. The Denali ice core drilling (DEN-13B) is indicated by the vertical blue line.



834

835 **Figure 3** Calibrated ^{14}C age probability distributions for samples from the Denali ice core
 836 (DEN-13B), as derived in OxCal v4.4.4 using the IntCal 20 radiocarbon calibration curve
 837 (Ramsey 2021, Reimer et al. 2020). Light green areas indicate the priori age probabilities, the
 838 dark green areas the posterior probabilities when sequential ordering of samples is assumed
 839 (see main text). The Agreement Index (A) indicates overlap between these two probability
 840 functions. A value < 60 indicates poor agreement (see main text). The 1σ and 2σ range is
 841 indicated by the lines below the probability distribution areas.

842

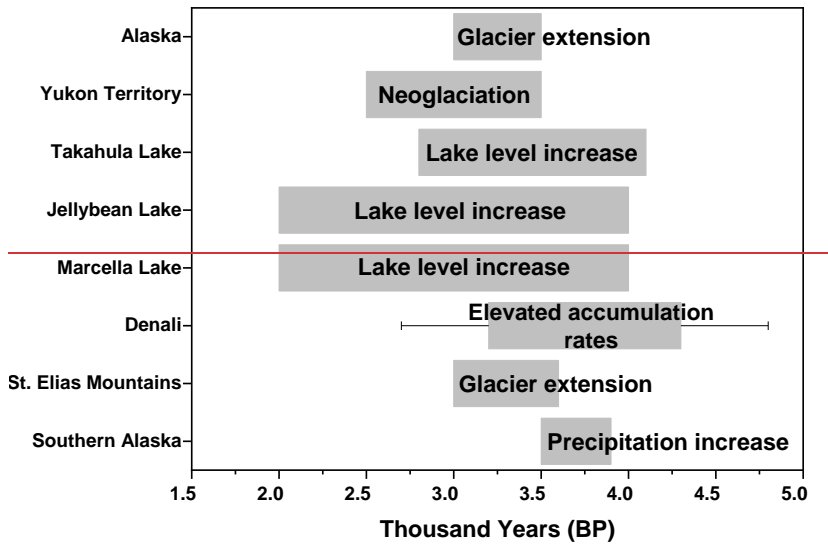


843

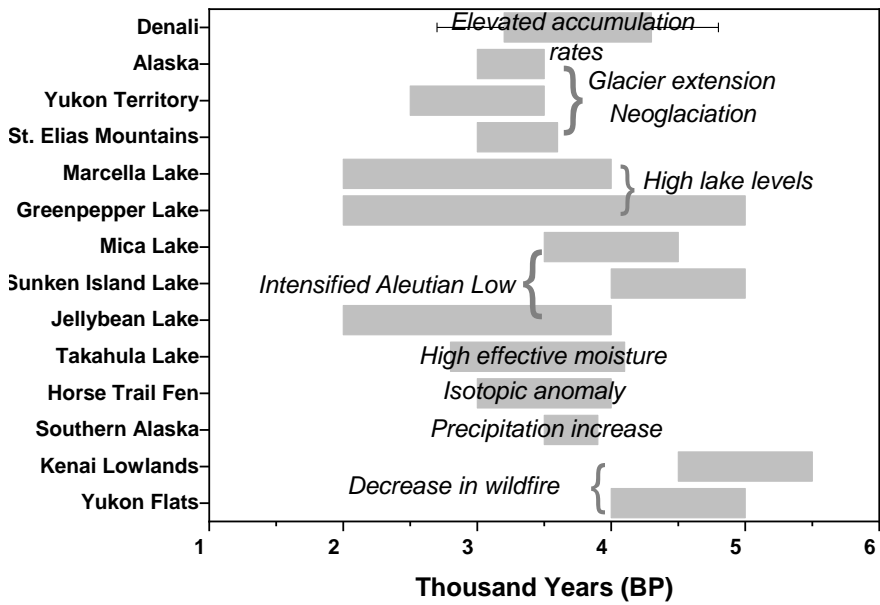
844 **Figure 4** Denali ice core (DEN-13B): annual layer counting (ALC), dating horizons (^{14}C ,
 845 Volcanos, ^{137}Cs peak) and modeled, continuous age-depth relationship (1D ice flow model, see
 846 main text). (a) Model output for constant accumulation rates (b , in m w.e. yr^{-1}). (b) Modeled
 847 age-depth relationship for variable b (inverse model). (c) Zoom of the deepest part. All error
 848 bars indicate the 1σ uncertainty.

849

850



851



852

域代码已更改

853 **Figure 5** Regional paleoclimate changes as reported in previous studies (~~L.~~ Anderson et al.
854 ~~2005a, 2005ba, 2005b, 2016, 2019, R.S. Anderson et al. 2006, Broadman et al. 2020,~~ Clegg
855 and Hu 2010, Denton and Karlén 1977, Heusser et al. 1985, ~~Jones et al. 2019, Kelly et al. 2013,~~
856 ~~Schiff et al. 2009,~~ Solomina et al. 2015) and the period of elevated annual net accumulation
857 rates indicated in the Denali ice core DEN-13B (this study, see main text).

858

859

860